Bulletin of Faculty of Science, Zagazig University (BFSZU)
e-ISSN: 1110-1555
Volume-2024, Issue-1, pp-168-181
https://bfszu.journals.ekb.eg/journal
Research Paper DOI: 10.21608/bfszu.2023.234122.1306

==========

Investigating the Antioxidant Capacity of Ni(II) Complexes with febuxostat in the presence of 2,2′-bipyridine and paracetamol

Leila M. Abbass*, Sadeek A. Sadeek, Mohamed S. El-Attar, Wael A. Zordok

Department of Chemistry, Faculty of Science, Zagazig University, Zagazig, 44519, Egypt.
Corresponding author: magdyleila95@gmail.com

***ABSTRACT*: This article presents the synthesis of two nanoparticles Ni(II) complexes, $[Ni(FEB)(Bipy)(H_2O)_2]Cl.2H_2O$ and $[Ni(FEB)(Para)(H_2O)_2]Cl.5H_2O$ (FEB = febuxostat, Bipy = 2,2′-bipyridine, Para = paracetamol). Elemental analysis, magnetic moment (μeff), molar conductivity, XRD, mass spectrometry (MS), UV-visible, FT-IR and TG-DTG studies were utilized to determine the chemical formulae and structures of synthesized complexes. Results from the FT-IR study suggest FEB, Bipy and Para chelated with Ni(II) ion through OS, NN, NO, respectively, as bidentate ligands. μeff and electronic spectra results indicate the complexes have an octahedral geometry. XRD pattern showed the polycrystalline structure of complexes with crystalline sizes 83.42 and 38.84 nm, confirming nanostructure of complexes. The thermal stability of complexes was investigated with TG-DTG analysis. Coats-Redfern and Horowitz-Metzger equations were employed to determine the kinetic parameters of thermal decomposition stages. Lastly, in vitro antioxidant activities of FEB and complexes were evaluated by DPPH assay. The antioxidant activities test exposed that complex $[Ni(FEB)(Para)(H_2O)_2]Cl.5H_2O$ has higher activities than complex $[Ni(FEB)(Bipy)(H_2O)_2]Cl.2H_2O$.**

KEYWORDS: FEB, Ni(II) complexes, TG-DTG, XRD, antioxidant

Date of Submission: 04-09-2023 Date of acceptance: 24-09-2023

I. INTRODUCTION

Febuxostat**,** 2-(3-cyano-4-isobutyloxyphenyl)-4-methyl-5-thiazolecarboxylic acid (**FEB**) (Scheme 1a), serves as a type of urate-lowering medication used for the treatment of gout hyperuricemia [1,2]. **FEB** works by inhibiting xanthine oxidase, **FEB** impedes uric acid formation and disrupts the molybdenum pterin position on oxidized compounds [3,4]. Derivatives of thiazole carboxylic acids have garnered interest and this is due to the heterocyclic ring's association with the carboxyl group, which provides a number of coordination options [5,6]. Recent research suggests that Bipy (Scheme 1b) compounds can improve myocardial contractility and cause slight arterial dilation at a systemic level [7]. In addition, Bipy complexes have been successfully used in areas such as catalysis, analytical chemistry, biochemistry, energy transfer, supramolecular and material chemistries [8]. Due to their steadiness during redox reactions and simplification of functionalization, Bipy-generated ligands have been used quite extensively [8,9]. **Para** is 4-hydroxy acetanilide (Scheme 1c). The widespread usage of **Para** as a self-mediated analgesic is attributed to its ability to inhibit the cyclooxygenase (COX) pathway in the central nervous system, thereby hindering the production of prostaglandins, which are known to be pain mediators. Over the years, **Para** has proven to be the most popular anesthetic when it comes to natural pain relief. Additionally, its effects may extend to an improvement of endocannabinoid transmission and

modulation of descending serotonergic inhibitory pathways [11,12]. In the current work, we characterize new Ni(II) complexes of **FEB** in the presence of **Bipy** and **Para** by μ_{eff}, elemental analyses, FT-IR, molar conductivity, UV-vis., XRD and thermal analyses. The aim of the present work, study the effect of Ni(II) on the antioxidant efficiency of febuxostat in the presence of 2,2′-bipyridine and paracetamol.

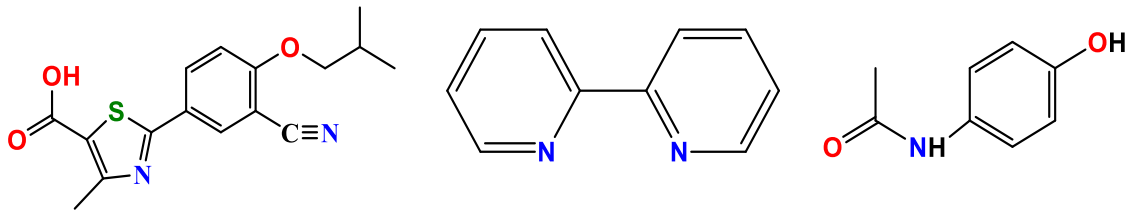

(a) (b) (c)

Scheme 1: (a) FEB, (b) Bipy and (c) Para.

II. MATERIALS AND METHODS

2.1. Materials and instruments

FEB and **Para** were gifts from Eva Pharma Pharmaceutical and Organo Pharma whereas ethanol, DMF, **Bipy**, $NiCl_2.6H_2O$ and $AgNO_3$, were from Sigma Aldrich Chemical Company. The solvents and materials were used without purification. All instrumentation used are discussed previously [5].

2.2. Synthesis of Ni(II) complexes

2.2.1. Synthesis of $[Ni(FEB)(Bipy)(H_2O)_2]Cl.2H_2O$

Mint solid complex was synthesized by combining 1 mmol of **FEB** (0.316 g) in 20 mL of ethyl alcohol and then adding 1 mmol of **Bipy** (0.156 g). Finally, 1 mmol of $NiCl_2.6H_2O$ was added to a stirred mixture drop-wise. The mixture was heated by reflux for 6 hrs. The precipitate was formed then isolated from the mixture and washed several times with ethanol which was vacuum-dried using anhydrous calcium chloride.

2.2.2. Synthesis of $[Ni(FEB)(Para)(H_2O)_2]Cl.5H_2O$

Grey solid complex was synthesized by combining 1 mmol of **FEB** (0.316 g) in 20 mL of ethyl alcohol and then adding 1 mmol of **Para** (0.151 g). Finally, 1 mmol of $NiCl_2.6H_2O$ was added to a stirred mixture drop-wise. The mixture was heated by reflux for 6 hrs. The precipitate was formed then isolated from the mixture and washed several times with ethanol which was vacuum-dried using anhydrous calcium chloride.

2.3. Antioxidant activity

Using ascorbic acid as the reference material by the DPPH assay, the antioxidant activity of **FEB** and Ni(II) complexes was determined [13]. The compounds were mixed with an equivalent amount of DPPH (0.135 mg/mL) and then, diluted with an equivalent amount of methanol. The samples were stored at ambient temperature in the absence of light for a period of 30 minutes and absorbance was measured at 517 nm. The radical scavenging activity (RSA) and inhibition percentage (PI) of DPPH were calculated using eqs. 1 and 2 [1,14].

$$PI = \frac{A_{control} - A_{complex}}{A_{control}} \times 100\ \% \qquad (1)$$

where, at t = 30 min, $A_{complex}$ = absorbance (DPPH + complex)

at t = 0 min, $A_{control}$ = absorbance (DPPH + methyl alcohol)

$$RSA = 100 - PI\ \% \quad (2)$$

RSA% values were charted in relation to the concentration (mg/mL) of compounds to calculate effective concentration (IC_{50}) [15].

III. RESULTS AND DISCUSSION

The synthesized Ni(II) complexes were non-hygroscopic, heat resistant at room temperature and slightly soluble in water, yet soluble in DMSO or DMF. Molar conductance of complexes (1×10^{-3} M) in DMF was found at 65.25 and 68.76 S cm^2 mol^{-1}, which revealed complexes were 1:1 electrolytes and complexes give white precipitate using $AgNO_3$ solution [16,17]. Elemental analysis data agreed with the expected molecular formulae of the examined Ni(II) chelates (Table 1). The percentage of Ni(II) ion: determined gravimetrically by transforming the solid products into NiO and also by using atomic absorption method. The chloride content in complexes were determined by using two method:1- Mohr's method: The complexes solution were estimated volumetrically according to Mohr method which is based on titration of chloride with standard solution of AgNO3 in the present of K2CrO4 as indicator and 2- Volhard's method: The complexes solution were estimated volumetrically according to back titration which involves an additional excess of AgNO3 to complex solution this excess is titrated against ammonium thiocyanate, with ferric ammonium sulphate as indicator.

Table 1: Elemental analysis and physico-analytical data for FEB, Bipy, Para and their metal complexes.

Compounds M.Wt. (M.F.)	Color Yield, %	M.P. °C	Calc. (Found) (%)					Λ Ω cm^2 mol^{-1}
			C	H	N	M	Cl	
FEB 316.00 ($C_{16}H_{16}N_2O_3S$)	White -	206	-	-	-	-	-	2.71
Bipy 156.00 ($C_{10}H_8N_2$)	White -	70	-	-	-	-	-	4.12
Para 151.00 ($C_8H_9NO_2$)	White -	169		-	-	-	-	2.58
[Ni(FEB)(Bipy)$(H_2O)_2$]Cl.2H_2O 637.19 ($NiC_{26}H_{31}N_4O_7SCl$)	Mint 87.58	208	48.84 (48.96)	4.82 (4.87)	8.70 (8.79)	9.07 (9.21)	5.50 (5.57)	65.25
[Ni(FEB)(Para)$(H_2O)_2$]Cl.5H_2O 686.19 ($NiC_{24}H_{38}N_3O_{12}SCl$)	Grey 84.73	190	41.84 (41.97)	5.48 (5.54)	6.06 (6.12)	8.46 (8.55)	5.11 (5.17)	68.76

3.1. FT-IR spectra

FT-IR spectra of **FEB**, **Bipy**, **Para** and complexes were presented in Figure 1. The coordination sites were identified by contrasting FT-IR data of complexes with free ligands (Table 2). In **FEB**, the presence of ν(C-S) at 1277, $\nu(C{=}O)_{COOH,}$ at 1677, $\nu(O\text{-}H)_{COOH}$ at 3470 and ν(C≡N) at 2231 cm^{-1} [18]. From spectra of complexes indicated the absence band of $\nu(C{=}O)_{COOH}$ at 1677 cm^{-1}. The observed of $\nu_{as}(COO^-)$ at 1683 and 1651 cm^{-1} while, $\nu_s(COO^-)$ at 1474 and 1424 cm^{-1}, with a difference of 209 and 227 cm^{-1} in complex

[Ni(FEB)(Bipy)$(H_2O)_2$]Cl.2H_2O and **[Ni(FEB)(Para)$(H_2O)_2$]Cl.5H_2O**, respectively, confirming that a monodentate type of carboxylate group [1,19,20]. The change ν(C-S) from 1277 to higher values (1292 and 1284 cm^{-1}) in complex **[Ni(FEB)(Bipy)$(H_2O)_2$]Cl.2H_2O** and **[Ni(FEB)(Para)$(H_2O)_2$]Cl.5H_2O**, respectively. confirming chelation through sulfur of thiazole ring (Scheme 2) [21]. The increase in the C-S bond's strength after coordination. Possible reduction in the electron repulsion between the sulphur lone pair and bound pair electrons, lead to a stronger C-S bond, which would subsequently lead to a higher bond frequency as a result coordination of C-S with metal ions

After complexation, **Bipy** ν(C=N) at 1578 shifted to a lower value (1514 cm^{-1}), showing that chelating via two nitrogen atoms of **Bipy** in the complexes [20,22,23]. For **Para**, the ν(C=O) and (N-H) bands, which were at 1645 and 3159 cm^{-1}, were moved to higher values, suggesting that C=O and N-H groups were engaged in the chelation process [24]. The new bands with different strengths for complex **[Ni(FEB)(Bipy)$(H_2O)_2$]Cl.2H_2O** were observed at 657 cm^{-1} for ν(M-O) and 420 cm^{-1} for (M-N). for complex **[Ni(FEB)(Para)$(H_2O)_2$]Cl**.5H_2O, at 614, 517 and 446 cm^{-1} for ν(M-O), ν(M-N) and ν(M-S), respectively [1,20].

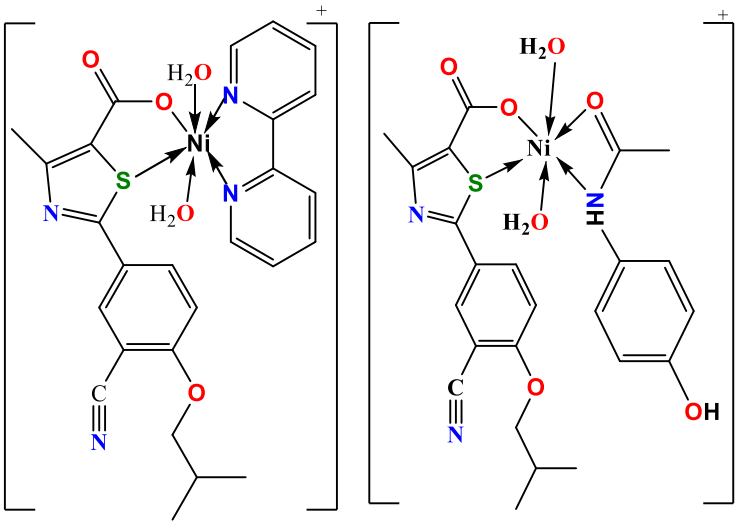

Scheme 2: Chelation mode of Ni(II) with mixed ligand

Table 2: Selected infrared spectra frequencies (cm^{-1}) of FEB, Bipy, Para and their metal complexes

Compounds	ν(O-H): COOH, phenolic, H_2O	ν(N-H)	ν(C=O); COOH	ν(C=O); Para	$\nu_{as}(COO^-)$	ν(C=N) Bipy	$\nu_s(COO^-)$	$\Delta\nu$ (ν_{as} - ν_s)	ν(C-S) thiazole	ν(M-X)
FEB	3470mbr	-	1677vs	-	-	-	-	-	1277s	-
Bipy	3440mbr	-	-	-	-	1578ms	-	-	-	-
Para	3321ms	3159m	-	1645s	-	-	-	-	-	-
[Ni(FEB)(Bipy)$(H_2O)_2$]Cl.2H_2O	3528ms 3439m 3329m	-	-		1683m	1514ms	1474ms	209	1292vs	657w 420w
[Ni(FEB)(Para)$(H_2O)_2$]Cl.5H_2O	3349m 3336m	3202br	-	1680ms	1651m	-	1424s	OOT	1284s	SNQw 517w 446w

Keys: s=strong, m=medium, v=very, w=weak, br=broad, *ν*=stretching.

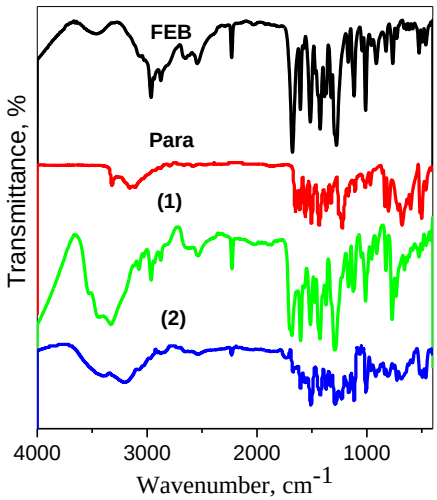

Figure 1: Infrared spectra of FEB, Para, complex (1) [Ni(FEB)(Bipy)$(H_2O)_2$]Cl.2H_2O and (2) [Ni(FEB)(Para)$(H_2O)_2$]Cl.5H_2O.

3.2. UV-vis. spectra

To obtain information on complex structure, the electronic spectra of **FEB**, **Para** and complexes were studied in the range of 200 to 800 nm using DMF (Figure 2). The bands at 293, 284 and 295 nm attributed to π→π* while, (330, 370), (347) and (310, 385) to n→π* transition in **FEB**, **Bipy** and **Para**, respectively (Table 3) [1]. For complex **[Ni(FEB)(Bipy)$(H_2O)_2$]Cl.2H_2O** and **[Ni(FEB)(Para)$(H_2O)_2$]Cl.5H_2O**, three bands at (24390, 19608 and 14925) cm^{-1} and (19607, 14925 and 14084) cm^{-1} assignable to $^3A_2g(F) \rightarrow {}^3T_1g(P)$, $^3A_2g(F) \rightarrow {}^3T_1g(F)$ and $^3A_2g(F) \rightarrow {}^3T_2g$ transitions in an octahedral structure with μ_{eff} values 2.92 and 2.96 B.M [1,25]. The values of 10Dq for complex **[Ni(FEB)(Bipy)$(H_2O)_2$]Cl.2H_2O** and **[Ni(FEB)(Para)$(H_2O)_2$]Cl.5H_2O** were 179 and 168 kJ/mol and crystal field stabilization energy (CFSE) -215+3p and -202+3P, respectively (Table 3).

Table 3: UV-vis. spectra for FEB, Bipy, Para and Ni(II) complexes

Compounds	π-π*and n-π* transitions, λmax (nm)	ν (cm^{-1})	Ligand-metal charge transfer λmax (nm)	ν (cm^{-1})	d-d transition λmax (nm)	ν (cm^{-1})	μ_{eff} (B.M.)
FEB	293 330, 370	34130 30303, 27027	-	-	-		-
Bipy	284 347	35211 28818	-	-	-		-
Para	295 310, 385	33898 32258, 25974	-	-	-		-
[Ni(FEB)(Bipy)$(H_2O)_2$]Cl.2H_2O	335 370	29851 27027	390	25641	410 510 670	24390 19608 14925	2.92
[Ni(FEB)(Para)$(H_2O)_2$]Cl.5H_2O	295 330, 390	33898 30303, 25641	470	21276	510 670 710	19607 14925 14084	2.96

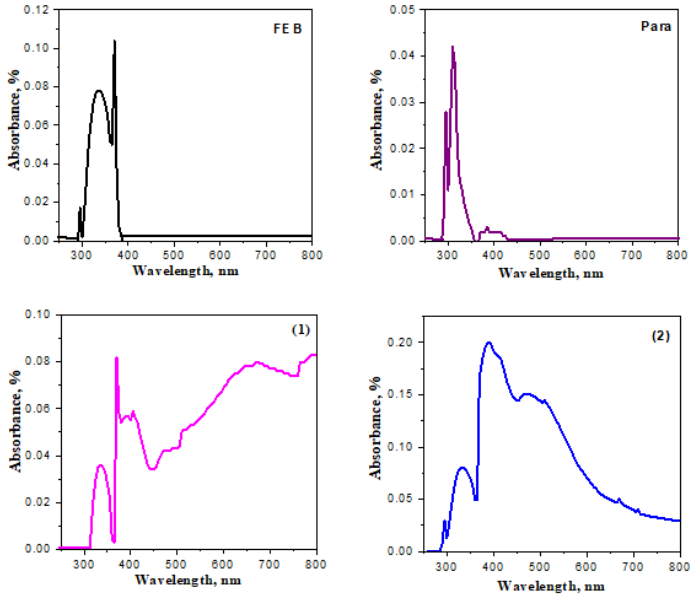

Figure 2: Electronic spectra for FEB, Para, complex (1) [Ni(FEB)(Bipy)$(H_2O)_2$]Cl.2H_2O and (2) [Ni(FEB)(Para)$(H_2O)_2$]Cl.5H_2O

3.3. Mass spectrometry (MS)

The molecular weights of complexes **[Ni(FEB)(Bipy)$(H_2O)_2$]Cl.2H_2O** and **[Ni(FEB)(Para)$(H_2O)_2$]Cl.5H_2O** were compared to their respective m/z values, confirming the predicted molecular formulas (Figure 3). The molecular ion peak measurements for complexes **[Ni(FEB)(Bipy)$(H_2O)_2$]Cl.2H_2O** and **[Ni(FEB)(Para)$(H_2O)_2$]Cl.5H_2O** were 637 and 686 amu.

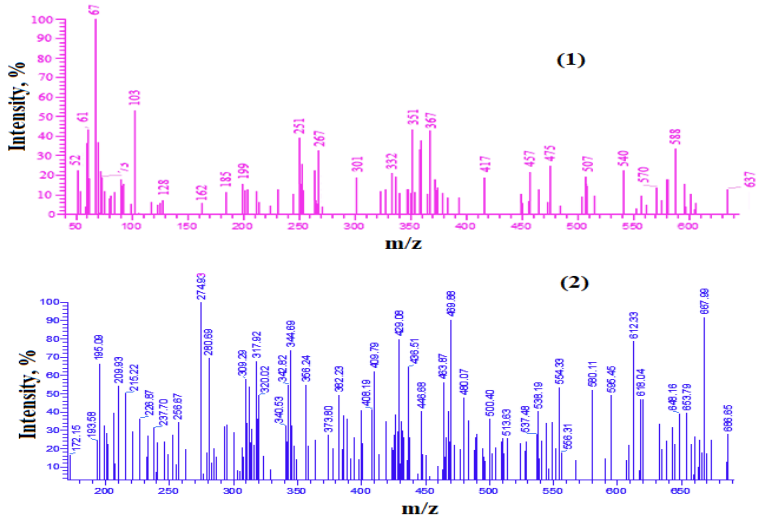

Figure 3: Mass spectrometry diagrams complex (1) [Ni(FEB)(Bipy)(H_2O)$_2$]Cl.2H_2O and (2) [Ni(FEB)(Para)(H_2O)$_2$]Cl.5H_2O.

3.4. Thermal analysis

The formulas of synthesized complexes may be strongly supported by TG, which is also employed to establish the found of H_2O molecules in inner or outer coordination sphere. Thermal analysis testing was used to study weight loss % and thermal stability of **FEB**, **Bipy, Para** and complexes (Table 4 and Figure 4). TG showed **FEB**, **Bipy** and **Para** decompose in one step at Tmax 292, 164 and 310 °C with loss weight 99.79, 99.64 and 99.18 % (calc. 100 %) related to loss $6C_2H_2$+2CO+H_2O+C_2N_2+H_2S, $4C_2H_2$+C_2N_2 and $4C_2H_2$+0.5H_2+NO_2. Complex **[Ni(FEB)(Bipy)(H_2O)$_2$]Cl.2H_2O** and **[Ni(FEB)(Para)(H_2O)$_2$]Cl.5H_2O** decomposed in three steps and the liberation of hydrated water present at 113 and 50 °C with weight loss 5.93 and 12.97 % (calc. 5.65 and 13.12 %), respectively. The second stage of decomposition is present at 269 °C for complex **[Ni(FEB)(Bipy)(H_2O)$_2$]Cl.2H_2O** and 167, 259 for complex **[Ni(FEB)(Para)(H_2O)$_2$]Cl.5H_2O**, this step is associated with loss 2H_2O+11C_2H_2+0.5Cl_2 and 3H_2O+0.5Cl_2+6C_2H_2+2CO+C_2N_2+H_2S, respectively. The third step was found at (387, 447, 492) and (484) °C for complexes **[Ni(FEB)(Bipy)(H_2O)$_2$]Cl.2H_2O** and **[Ni(FEB)(Para)(H_2O)$_2$]Cl.5H_2O** and leaving NiO+C and NiO as residue, respectively (Table 4).

Table 4: The maximum temperature T_{max} (°C) and weight loss values of the decomposition stages for FEB, Bipy, Para and Ni(II) complexes.

Compounds	Decomposition	T_{max}(°C)	Weight loss (%)		Lost species
			Calc.	Found	
FEB	1st Total loss	292	100 100	99.79 99.79	$6C_2H_2+2CO+H_2O+C_2N_2+H_2S$
Bipy	1st Total loss	164	100 100	99.64 99.64	$4C_2H_2+C_2N_2$
Para	1st Total loss	310	100 100	99.18 99.18	$4C_2H_2+0.5H_2+NO_2$
[Ni(FEB)(Bipy)$(H_2O)_2$]Cl.2H_2O	1st 2nd 3rd Total loss Residue	113 269 387, 447, 492	5.65 55.93 24.58 86.44 13.56	5.93 55.93 24.58 86.44 13.56	$2H_2O$ $2H_2O+11C_2H_2+0.5Cl_2$ $HSCN+2CO+1.5N_2$ NiO+C
[Ni(FEB)(Para)$(H_2O)_2$]Cl.5H_2O	1st 2nd 3rd Total loss Residue	50 167, 259 484	13.12 56.47 19.67 89.26 10.74	12.97 55.98 21.00 89.95 10.05	$5H_2O$ $3H_2O+0.5Cl_2+6C_2H_2+2CO+C_2N_2+H_2S$ $4C_2H_2+NO+0.5H_2$ NiO

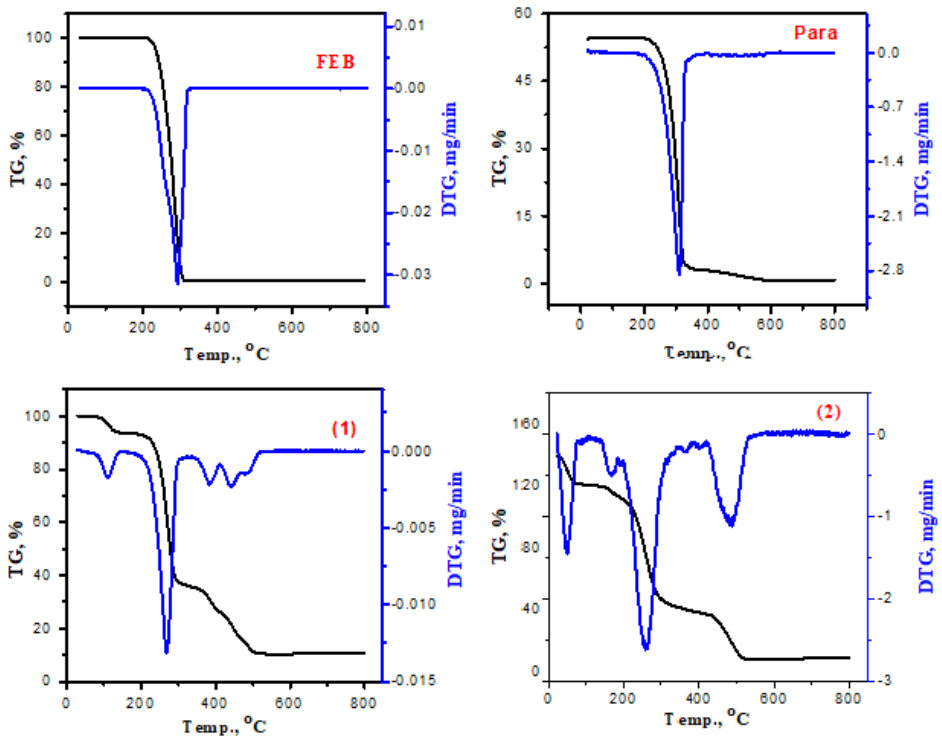

Figure 4: TG and DTG diagrams for FEB, Para, complex (1) [Ni(FEB)(Bipy)$(H_2O)_2$]Cl.2H_2O and (2) [Ni(FEB)(Para)$(H_2O)_2$]Cl.5H_2O.

3.5. Thermodynamic and kinetic parameters

Using Coats-Redfern and Horowitz-Metzger equations, the thermodynamic parameters were calculated (Table 5 and Figure 5). Free energy changes (ΔG*), entropy (ΔS*), activation energy (E_a) and Enthalpy (ΔH*) of our compounds **[**26,27**].** Positive ΔH* values show that processes are endothermic and higher E_a values show the more thermally stable complexes [28]. Negative ΔS* values of complexes indicate that they are more activated [25]. The positive values of ΔG* indicated that metal ions work autocatalytically to accelerate both non-spontaneous processes and the thermal breakdown of synthesized complexes [25,26].

Table 5: Kinetic and thermal behavior parameters for FEB, Bipy, Para, complex (1) [Ni(FEB)(Bipy)$(H_2O)_2$]Cl.2H_2O and (2) [Ni(FEB)(Para)$(H_2O)_2$]Cl.5H_2O

Compounds	Decomposition range (K)	T_s (K)	Method	Parameter					R^a	SD^b
				E^* (kJ/mol)	A (s^{-1})	ΔS^* (kJ/mol.K)	ΔH^* (kJ/mol)	ΔG^* (kJ/mol)		
FEB	477-606	565	CR HM	174.15 177.53	1.78×10^{14} 2.88×10^{14}	0.023 0.027	169.46 172.83	156.70 157.55	0.981 0.950	0.522 0.809
Bipy	315-554	437	CR HM	75.70 95.74	6.53×10^{6} 2.79×10^{9}	-0.1176 -0.0672	72.06 92.11	123.46 121.49	0.998 0.998	0.094 0.106
Para	475-640	583	CR HM	102.84 108.29	8.18×10^{6} 5.35×10^{7}	-0.118 -0.102	98.10 103.55	165.46 161.99	0.997 0.991	0.085 0.139
(1)	198-315	542	CR HM	173.15 183.34	3.06×10^{11} 1.02×10^{12}	-0.029 -0.038	168.64 178.64	184.89 157.40	0.989 0.983	0.315 0.420
(2)	473-626	532	CR HM	43.18 36.31	0.57×10^{2} 0.09×10^{2}	-0.216 -0.231	38.76 31.88	153.76 154.82	0.992 0.995	0.095 0.032

a= Arrhenius correlation coefficients and b=standard deviation

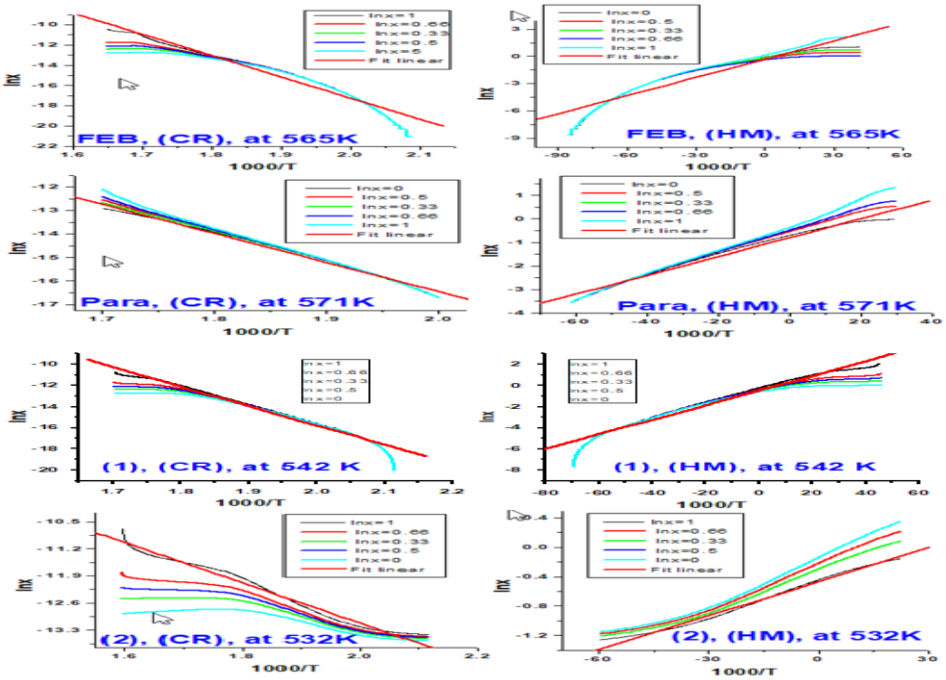

Figure 5: The kinetic parameters diagrams of FEB, Para, complex (1) [Ni(FEB)(Bipy)$(H_2O)_2$]Cl.2H_2O and (2) [Ni(FEB)(Para)$(H_2O)_2$]Cl.5H_2O.

3.5. X-ray diffraction

Using Debye-Scherer eqs. 3-5, X-ray diffraction was used to identify the crystallite size (Cs), dislocation density (D), and micro strain (ε) of **FEB, Bipy, Para,** and complexes Table 6 and Figure 6.

$$Cs = \frac{K\lambda}{\beta\cos\theta} \qquad (3)$$

$$D = \frac{1}{C_s^2} \qquad (4)$$

$$\varepsilon = \frac{\beta}{4\tan\theta} \qquad (5)$$

Where k = 0.94, λ = 1.5406 Å, diffraction angle (θ) and full width at half maximum (FWHM) of diffracted peak (β) [29]. Table 6 summarizes the results of the calculations, which showed nanostructures for compounds, with C_s values 83.51, 71.10, 66.32, 83.42 and 38.84, for **FEB**, **Bipy**, **Para** and complexes respectively. The D values were found at (1.43, 1.98, 2.27, 1.44 and 6.63) × 10^{-4} nm^{-2} for **FEB**, **Bipy**, **Para** and complexes, respectively [30]. ε values were (38.15, 34.47, 25.81, 41.97 and 83.50) × 10^{-4} rad, respectively, for **FEB**, **Bipy**, **Para** and complexes.

Table 6: From XRD pattern, (C_s, D and ε) of FEB, Bipy, Para and Ni(II) complexes determined

Compounds	2θ (º)	d value (Aº)	FWHM	C_s (nm)	D (δ) × 10^{-4}, (nm^{-2})	ε × 10^{-4}
FEB	13.05	6.78	0.100	83.51	1.43	38.15
Bipy	16.99	5.22	0.118	71.10	1.98	34.47
Para	24.42	3.64	0.128	66.32	2.27	25.81
[Ni(FEB)(Bipy)(H_2O)$_2$]Cl.2H_2O	11.87	7.450	0.100	83.42	1.44	41.97
[Ni(FEB)(Para)(H_2O)$_2$]Cl.5H_2O	12.822	6.90	0.215	38.84	6.63	83.50

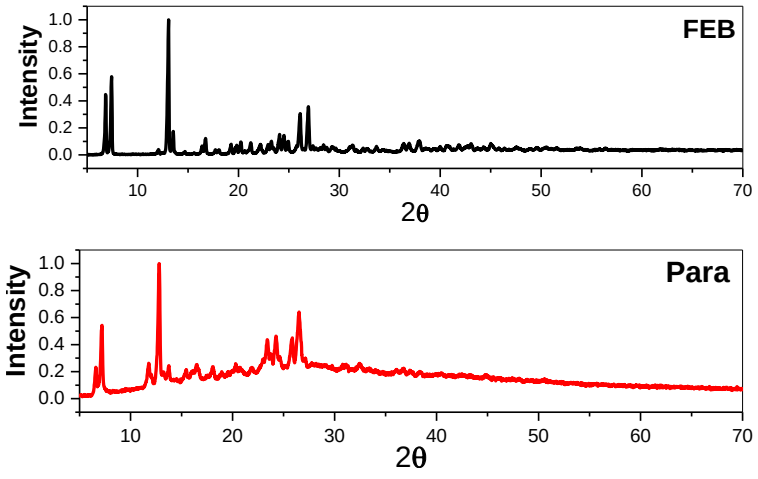

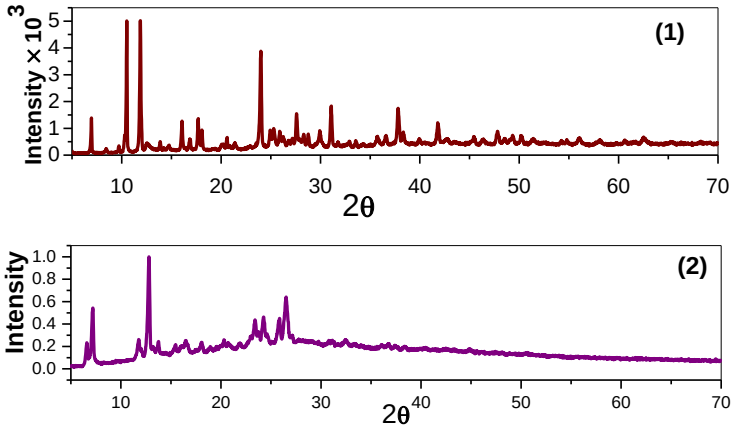

Figure 6 XRD pattern for FEB, Para, complex (1) [Ni(FEB)(Bipy)$(H_2O)_2$]Cl.2H_2O and (2) [Ni(FEB)(Para)$(H_2O)_2$]Cl.5H_2O.

3.6. DPPH antioxidant activity

The results from comparing DPPH free radical scavenging activity of complex **[Ni(FEB)(Bipy)$(H_2O)_2$]Cl.2H_2O** and **[Ni(FEB)(Para)$(H_2O)_2$]Cl.5H_2O** to ascorbic acid are represented in Table 7 and Figure 7. The results demonstrated that complex **[Ni(FEB)(Para)$(H_2O)_2$]Cl.5H_2O** was the stronger radical scavenger than complex **[Ni(FEB)(Bipy)$(H_2O)_2$]Cl.2H_2O**, exhibiting IC_{50} 0.436 and 2.234 mg/mL, respectively. Additionally, as IC_{50} values decreased, the complexes' ability to scavenge DPPH free radical was observed to increase. Compared to ascorbic acid, **FEB** and complex **[Ni(FEB)(Para)$(H_2O)_2$]Cl.5H_2O** had the most effective scavenging ability, indicated by their lowest IC_{50} values of 0.124 and 0.436 mg/mL.

Table 7: The antioxidant results of FEB and complexes

Compounds	Concentrations (mg/mL)	PI	RSA	IC_{50}, mg/mL
FEB	0.260	39.26	60.74	0.124
	0.130	43.12	56.88	
	0.065	56.88	43.12	
	0.033	65.76	34.24	
[Ni(FEB)(Bipy)$(H_2O)_2$]Cl.2H_2O	2.083	52.87	47.13	2.234
	1.042	60.03	39.97	
	0.521	68.34	31.66	
	0.260	77.65	22.35	
[Ni(FEB)(Para)$(H_2O)_2$]Cl.5H_2O	2.088	26.64	73.36	0.436
	1.044	32.5	67.5	
	0.522	48.85	51.15	
	0.261	58.79	41.21	
Ascorbic acid	0.062	15.267	85.19	0.022
	0.031	39.084	62.07	
	0.016	61.069	40.74	
	0.008	74.809	27.41	

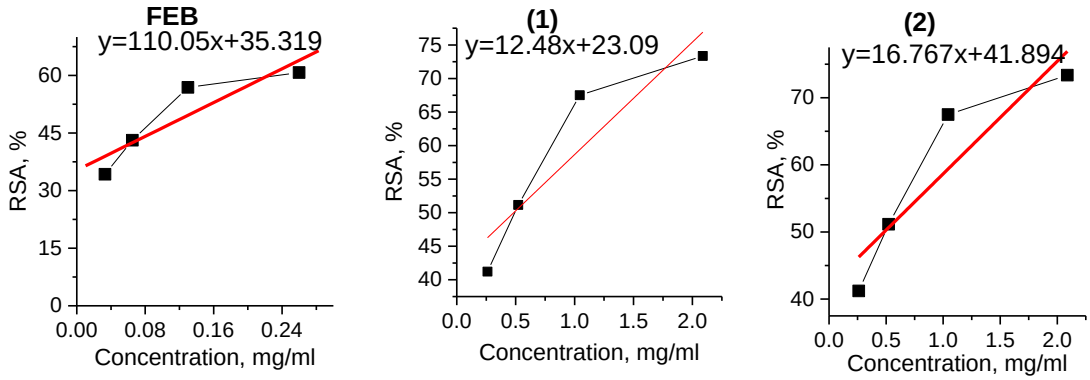

Figure 7: RSA % of FEB and complex (1) [Ni(FEB)(Bipy)(H_2O)$_2$]Cl.2H_2O and (2) [Ni(FEB)(Para)(H_2O)$_2$]Cl.5H_2O. using DPPH method.

V –CONCLUION

The isolated nanoparticles Ni(II) complexes of mixed ligand were synthesized and examined using a variety of techniques. complexes are colored and stable to air and temperature. Ni(II) complexes were found to have an octahedral structure according to UV-visible and µeff data. The FT-IR data revealed that FEB, Bipy and Para behave as bidentate ligands, in FEB through oxygen of carboxylate group and sulfur of thiazole ring, in Bipy through two nitrogens of pyridyl ring while, nitrogen and oxygen of amide group in Para. TG showed FEB, Bipy and Para decompose in one step and complex [Ni(FEB)(Bipy)(H2O)2]Cl.2H2O and [Ni(FEB)(Para)(H2O)2]Cl.5H2O decompose in three steps. Positive ΔH* values show that processes are endothermic and higher Ea values show the more thermally stable complexes. The positive values of ΔG*indicated that metal ions work autocatalytically to accelerate both non-spontaneous processes and the thermal breakdown of synthesized complexes The antioxidant activities test exposed that complex [Ni(FEB)(Para)(H2O)2]Cl.5H2O has higher activities than complex [Ni(FEB)(Bipy)(H2O)2]Cl.2H2O.

REFERENCES

1. Hosny, N. M., Atia, N. N., El-Gizawy, S. M. (2019): A review on: Analysis of certain drugs used in gout treatment. Microchemical Journal, 149, 103955.
2. Yu, K. H. (2007): Febuxostat: a novel non-purine selective inhibitor of xanthine oxidase for the treatment of hyperuricemia in gout. Recent patents on inflammation & allergy drug discovery, 1(1), 69-75.
3. Chinchilla, S. P., Urionaguena, I., Perez-Ruiz, F. (2016): Febuxostat for the chronic management of hyperuricemia in patients with gout. Expert Review of Clinical Pharmacology, 9(5), 665-673.
4. Al-adilee, K. J., Hessoon, H. M. (2019): Synthesis, spectral properties and anticancer studies of novel hetrocyclic azo dye ligand derived from 2-amino-5-methyl thiazole with some transition metal complexes. In Journal of Physics, Conference Series, 1234(1), 012094.
5. Salem, A. E., Mohammed, S. F., Sadeek, S. A., Zordok, W. A., El-Attar, M. S. (2022): Synthesis, structural elucidation, molecular modeling, and antimicrobial studies of some nanoparticles mixed ligands complexes of cetirizine in presence of 2, 2′-bipyridine. Applied Organometallic Chemistry, 36(7), e6715.
6. Jayamani, A., Bellam, R., Gopu, G., Ojwach, S. O., Sengottuvelan, N. (2018): Copper (II) complexes of bidentate mixed ligands as artificial nucleases: Synthesis, crystal structure, characterization and evaluation of biological properties. Polyhedron, 156, 138-149.
7. Gordon, S. G., Kittleson, M. D. (2008): Drugs used in the management of heart disease and cardiac arrhythmias. Small animal clinical pharmacology, 380-457.
8. Muthusamy, S., Natarajan, R. (2016): Pharmacological activity of a few transition metal complexes: A short review. Journal of Chemical Biology & Therapeutics, 1(2), 1-17.
9. Fadl, A. M., Sadeek, S. A., Magdy, L., Abdou, M. I., El-Shiwiniy, W. H. (2021): Multi-functional epoxy composite coating incorporating mixed Cu (II) and Zr (IV) complexes of metformin and 2, 2\-bipyridine as intensive network cross-linkers exhibiting anti-corrosion, self-healing and chemical-resistance performances for steel petroleum platforms. Arabian Journal of Chemistry, 14(10), 103367.

10. Abdel Shaheed, C., Ferreira, G. E., Dmitritchenko, A., McLachlan, A. J., Day, R. O., Saragiotto, B., Maher, C. G. (2021): The efficacy and safety of paracetamol for pain relief: an overview of systematic reviews. Medical Journal of Australia, 214(7), 324-331.
11. Wastesson, J. W., Martikainen, J. E., Zoëga, H., Schmidt, M., Karlstad, Ø., Pottegård, A. (2018): Trends in use of paracetamol in the Nordic countries. Basic & Clinical Pharmacology & Toxicology, 123(3), 301-307.
12. Sharma, C. V., Mehta, V. (2014): Paracetamol: mechanisms and updates. Continuing Education in Anaesthesia Critical Care & Pain, 14(4), 153-158.
13. Kitts, D. D., Wijewickreme, A. N., Hu, C. (2000): Antioxidant properties of a North American ginseng extract. Molecular and cellular biochemistry, 203, 1-10.
14. El-Gammal, O. A., Mohamed, F. S., Rezk, G. N., & El-Bindary, A. A. (2021): Structural characterization and biological activity of a new metal complexes based of Schiff base. Journal of Molecular Liquids, 330, 115522.
15. Parejo, I., Codina, C., Petrakis, C., Kefalas, P. (2000): Evaluation of scavenging activity assessed by Co (II)/EDTA-induced luminol chemiluminescence and DPPH (2, 2-diphenyl-1-picrylhydrazyl) free radical assay. Journal of Pharmacological and toxicological Methods, 44(3), 507-512.
16. Geary, W. J. (1971): The use of conductivity measurements in organic solvents for the characterisation of coordination compounds. Coordination Chemistry Reviews, 7(1), 81-122.
17. Al Zoubi, W., Nashrah, N., Putri, R. A. K., Allaf, A. W., Assfour, B., Ko, Y. G. (2022): Strong dual-metal-support interactions induced by low-temperature plasma phenomenon. Materials Today Nano, 18, 100213.
18. Kini, A., Patel, S. B. (2017): Phase behavior, intermolecular interaction, and solid state characterization of amorphous solid dispersion of Febuxostat. Pharmaceutical development and technology, 22(1), 45-57.
19. Abbass, L. M., Sadeek, S. A., Zordok, W. A., El-Telbany, M., El-Shwiniy, W. H. (2021): Synthesis, Structure, DFT, and Biological Activity of Metal Complexes of Norfloxacin and Metformin Mixed Ligand. Russian Journal of General Chemistry, 91, 1774-1782.
20. Kamal, H. M., El-Sayed, H. A., Sadeek, S. A., Zordok, W. A. A., El-Attar, M. S. (2023): Spectroscopic characterization, DFT modeling and antimicrobial studies of some novel nanoparticles mixed ligand complexes of NS bidentate ligand in presence of 2, 2′-bipyridine. Journal of Molecular Liquids, 376, 121404.
21. Masoud, M. S., Ali, A. E., Elasala, G. S., Amer, G. E. (2018): Ligating, Spectral and Thermal Properties of Febuxostat Metal Complexes. Journal of Chemical and Pharmaceutical Research, 10(7), 198-210.
22. Abebe, A., Kendie, M., Tigineh, G. T. (2021): Mono-and binuclear cobalt (II) mixed ligand complexes of 2, 2′-bipyridine and ethylenediamine: synthesis, characterization and biological application. Biointerface Research in Applied Chemistry, 12(2), 1962.
23. Tang, K., Zhang, J., Ren, N., Zheng, J., Liu, J., Wu, K. (2012): Crystal structures and thermal decomposition kinetics of lanthanide complexes with 3, 4, 5-trimethoxybenzoic acid and 1, 10-phenanthroline. Science China Chemistry, 55, 1283-1293.
24. Refat, M. S., Mohamed, G. G., El-Sayed, M. Y., Killa, H. M., & Fetooh, H. (2017): Spectroscopic and thermal degradation behavior of Mg (II), Ca (II), Ba (II) and Sr (II) complexes with paracetamol drug. Arabian Journal of Chemistry, 10, S2376-S2387.
25. Younis, A. M., El-Gamil, M. M., Rakha, T. H., Abu El-Reash, G. M. (2021): Iron (III), copper (II), cadmium (II), and mercury (II) complexes of isatin carbohydrazone Schiff base ligand (H3L): Synthesis, characterization, X-ray diffraction, cyclic voltammetry, fluorescence, density functional theory, biological activity, and molecular docking studies. Applied Organometallic Chemistry, 35(7), e6250.
26. Coats, A. W., Redfern, J. P. (1964): Kinetic parameters from thermogravimetric data. Nature, 201(4914), 68-69.

27. Horowitz, H. H., Metzger, G. (1963): A new analysis of thermogravimetric traces. Analytical chemistry, 35(10), 1464-1468.
28. Younis, A. M., Rakha, T. H., El-Gamil, M. M., El-Reash, G. M. A. (2022): Synthesis and Characterization of Some Complexes Derived from Isatin Dye Ligand and Study of their Biological Potency and Anticorrosive Behavior on Aluminum Metal in Acidic Medium. Journal of Inorganic and Organometallic Polymers and Materials, 32, 895.
29. Desoky, W. M., Dawood, M. S., El-Nahass, M. M. (2019): Structural, optical properties and junction characteristics, Au/n-KDDQ/p-Si/Al, of potassium-2, 3-dicyano-5, 6-dichloro-1, 4-benzo-quinone (KDDQ) films. Optik, 182, 1053-1063.
30. El-Nahass, M.M., W.M. Desoky. (2017): Investigating the structural and optical properties of thermally evaporated 1, 3, 3-trimethylindolino-b-naphthopyryl